

Journal of Materials Chemistry A

Accepted Manuscript



This is an *Accepted Manuscript*, which has been through the Royal Society of Chemistry peer review process and has been accepted for publication.

Accepted Manuscripts are published online shortly after acceptance, before technical editing, formatting and proof reading. Using this free service, authors can make their results available to the community, in citable form, before we publish the edited article. We will replace this *Accepted Manuscript* with the edited and formatted *Advance Article* as soon as it is available.

You can find more information about *Accepted Manuscripts* in the [Information for Authors](#).

Please note that technical editing may introduce minor changes to the text and/or graphics, which may alter content. The journal's standard [Terms & Conditions](#) and the [Ethical guidelines](#) still apply. In no event shall the Royal Society of Chemistry be held responsible for any errors or omissions in this *Accepted Manuscript* or any consequences arising from the use of any information it contains.

COMMUNICATION

Applications of ytterbium in inverted organic photovoltaic cells as high-performance and stable electron transport layers

Cite this: DOI: 10.1039/x0xx00000x

Received 00th January 2012,
Accepted 00th January 2012Gyu Min Kim^a, Il Soo Oh^a, Ae Na Lee^a, Se Young Oh^{*a}

DOI: 10.1039/x0xx00000x

www.rsc.org/

The electron transport layer (ETL) increases the power conversion efficiency (PCE) in organic photovoltaic cells (OPVs) by promoting the formation of ohmic contact between the active layer and the cathode metal. Here, we introduce ytterbium (Yb) as the electron transport layer in inverted OPVs where Yb is evaporated directly onto indium tin oxide (ITO). The inverted OPVs composed of ITO/Yb/P3HT:PCBM/MoO₃/Ag recorded PCEs of up to 4.3%, achieving 71% of the fill factor (FF) in one sun irradiation. Over 80% of its original PCE was retained after 30 days. The results indicate that Yb in inverted OPVs is vastly superior to other ETLs as it improves the majority of the parameters including short circuit current, FF and PCE. In this report, we will discuss the physical and optical functions of Yb in inverted OPVs which make Yb a promising candidate for simultaneously achieving a high PCE and good air stability.

Introduction

The development of organic photovoltaic cells (OPVs) has been an outstanding breakthrough which provides an innovative method for developing sustainable energy resources. Though OPVs have only recently become items of attention, they have already been seen to achieve a power conversion efficiency (PCE) in the range of 9.2% and 10.6% in single and tandem cells, respectively, exceeding the market entry barrier of PCEs which stands at 10%.¹⁻³ With the advent of the inverted OPV where ITO is most commonly used as a cathode, air stability has significantly improved as the anode which is not easily oxidized is located on the top side of OPV in inverted structures.⁴⁻⁷

^aSchool of Chemical and biomolecular Engineering, Sogang University, Seoul 121-742, South Korea

TiO_x or ZnO have been widely used as the electron transport layers (ETLs), altering the effective work function of ITO in inverted OPVs.⁸⁻⁹ However, there are several issues associated with inverted OPVs such as a lower PCE and a greater need for light absorption compared to conventional OPVs.¹⁰⁻¹²

One of the key challenges in overcoming the intrinsic defects in inverted OPVs is developing new ETLs which can improve performance. Recent studies in ETLs have suggested that polyelectrolytes such as polyethyleneimine (PEI) are extremely effective as ETLs in inverted OPVs.¹³⁻¹⁵ Synthesizing newly designed polymers could also lead to the rise of other effective ETLs.¹ On the other hand, there have been only a limited number of studies regarding the usage of raw metallic elements as ETLs in inverted OPVs. This is quite contrary to conventional OPVs where metallic elements such as Calcium (Ca), Magnesium (Mg) and Lithium (Li) are prevalently used as ETLs.¹⁶⁻¹⁷

Yb, a metallic element, was chosen originally in organic light emitting diodes (OLEDs) as an electron injection layer (EIL).¹⁸⁻¹⁹ However, only a few studies have been conducted regarding the application of Yb in conventional OPVs. Herein, we develop, for the first time, inverted OPVs featuring Yb as effective ETLs. Although most metallic elements are not suitable for inverted OPVs due to their poor performance, the use of Yb as an ETL results in outstanding developments with respect to the PCE and air stability, even superior to the use of PEI. Based on the physical performance of Yb, this paper seeks to further analyze and demonstrate the use of Yb in inverted OPVs.

Experiment

Reagents and materials

Regioregular poly (3-hexylthiophene-2,5-diyl) was purchased from Aldrich Co., Ltd. [6,6]-Phenyl-C61-butyracacidmethylester

(PC60BM) was purchased from Nano-C Co., Ltd. Poly (styrenesulfonate) complex was purchased from Bayer Co., Ltd. Other chemicals were used as reagent grades.

Fabrication of photovoltaic cells

The inverted OPV with Yb

Organic photovoltaic cells composed of ITO(2000Å)-Yb/P3HT:PCBM(2100Å)/MoO₃(50Å)/Ag were fabricated. Before the deposition of each layer, a patterned ITO ($\leq 20 \Omega/\square$) glass substrate was immersed into ultrasonic baths of deionized water, of acetone and of isopropyl alcohol for 15 minutes, for each solvent respectively. The cleaned ITO glass substrate was then dried at 80 °C for 60 minutes in a vacuum oven. After 15 minutes of UV-ozone treatment, the cleaned ITO was transferred to an evaporation chamber (ULVAC VTR-300M/1ERH evaporator, Japan). A thin layer of Yb was deposited in the vacuum chamber under 10^{-6} torr. After evaporating the Yb on the ITO, the sample was transferred to a glove box where a solution of P3HT:PCBM (1:1) in dichlorobenzene (36 mg/ml) was spin-casted onto the Yb on the ITO. This sample was then dried at 120°C for 10 minutes after slow growth where the sample was put in a petri dish for 1 hour. Finally, the MoO₃ (50Å) and silver were subsequently deposited onto the sample in the vacuum chamber. Electrical measurements and stability measurements developed were conducted under ambient conditions without encapsulation being disconnected from the load.

The inverted OPV with LiF

Cleaning procedures before the deposition of LiF are same as the procedures of OPV with Yb. After cleaning the ITO, the cleaned ITO was transferred to an evaporation chamber (ULVAC VTR-300M/1ERH evaporator, Japan). A thin layer of LiF was deposited in the vacuum chamber under 10^{-6} torr. The sample was transferred to the glove box to apply an active layer coating. The procedures after the deposition of LiF are same as the procedures for OPV with Yb.

The inverted OPV with PEIE

For the cells with polyethyleneimine-ethoxylated (PEIE), PEIE (1 ml) was diluted with 2-methoxyethanol (100 ml) and stirred for 30 minutes. Then, the diluted PEIE was spin-coated onto the cleaned ITO at 5000 rpm for 1 minute and thermally annealed for 10 minutes at 120 °C. The procedure after coating PEIE on the ITO is the same as the procedures for OPV with Yb.

The inverted OPV with amorphous titanium oxide (TiO_x)

The method to synthesize the sol-gel of TiO_x is detailed elsewhere.⁸ Sol-gel of TiO_x (0.5 ml) was diluted with ethanol (100 ml). On the cleaned ITO surface, the Sol-gel of TiO_x mixed with ethanol was spin-coated at 4000 rpm for 1 minute and annealed at 120 °C for 10 minutes. It was then transferred to a glove box to apply an active layer coating. The procedures after the deposition of TiO_x are the same as the procedures for OPV with Yb.

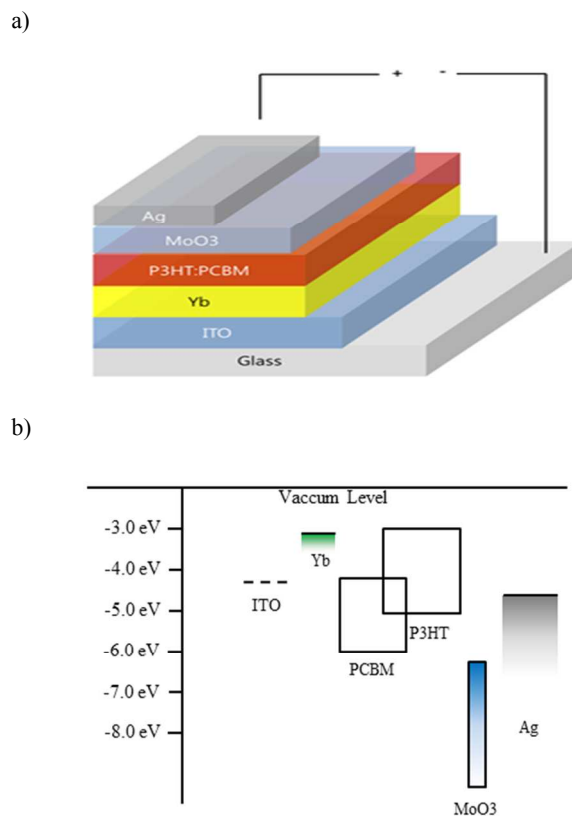


Fig. 1 (a) The cell structure of the inverted OPV using Yb (b) Energy diagram of the inverted OPV composed of ITO/Yb/P3HT:PCBM:MoO₃/Ag

Results and discussion

Properties of Yb

The cell structure of the inverted OPV using Yb is depicted in Fig. 1(a). In this inverted structure, Yb acts as the ETL on the ITO. Using ultraviolet photoelectron spectroscopy (UPS) analysis, we found the effective work function of Yb (2nm) on the ITO (see ESI Fig. S1) to be 3.14 eV, implying that Yb formed ohmic contact with the [6,6]-phenyl C61 butyric acid methyl ester (PCBM). This is because the work function of Yb was positioned above the lowest unoccupied molecular orbital (LUMO) level of PCBM.²⁰⁻²¹ We also confirmed the formation of ohmic contact between the ITO and Yb by using the current-voltage curve of the cell composed of ITO/Yb/Ag (see ESI, Fig. S2). These results indicate that the use of Yb in the inverted OPV as an ETL is viable.

Having considered the intrinsic properties of Yb on ITO, we investigated the current density-voltage (J-V) characteristics of inverted OPVs with varying thicknesses of Yb under 1 sun illumination (simulated AM 1.5G irradiation at 100mWcm⁻²) (see ESI, Fig. S3). The PCE increased substantially from 2.8% to 4.15% when the Yb thickness was increased by up to 2 nm (see ESI, Table S1). We assessed that the improvement in PCE after the increase in Yb thickness was caused by changes in the surface roughness of the ITO as Yb smoothens the ITO surface. The low surface roughness leads to a decrease in series resistances and also prevents short

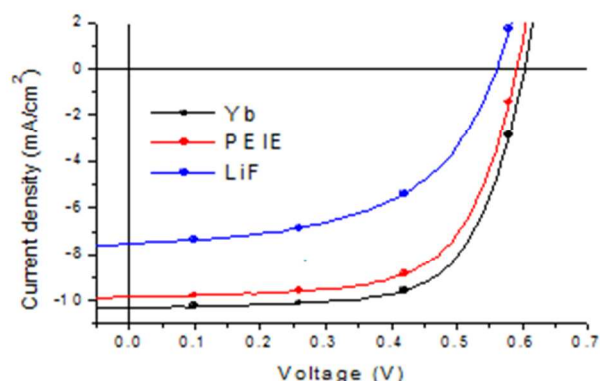


Fig. 2 J-V curves for the inverted OPVs with several ETLs: Yb, PEIE and LiF

circuiting (see ESI, Fig. S6). However, further increases of Yb thickness in inverted OPVs are detrimental to the PCE due to the increase in series resistances resulting from the insulating properties of Yb (see ESI, Fig. S2).

We compared the J-V curves of inverted OPVs with Yb to the J-V curves of other inverted OPVs with different ETLs (PEIE, LiF) (Fig. 2). The use of Yb as an ETL in conventional OPV is not as promising as the use of Yb in inverted OPVs. This is because conventional OPVs with Yb recorded values of PCE similar to those of conventional OPVs with other ETLs such as LiF and Ca (see ESI, Fig. S4). Introducing Yb as an ETL in inverted OPVs, however, gave rise to notable enhancements in the PCE which reached 4.15%, a result even superior to those of inverted OPVs using polyethyleneimine (PEIE) or LiF, which had PCEs of 3.61% and 2.27% respectively. Note that the inverted OPV with LiF in these experiments had also been optimized with various thicknesses (see ESI, Fig. S5). The PCE improvements of the cells with Yb are attributed to the improvements in J_{sc} and FF. To understand the mechanism of these improvements, we extracted the series resistances (R_s) and parallel resistances (R_p) (Table 1) using equivalent circuit models of photovoltaic cells,

$$J = J_{ph} - J_0 \left(e^{\frac{q(V+JAR_s)}{nkT}} - 1 \right) - \frac{V+JAR_s}{R_{sh}} \quad (1)$$

where J_{ph} corresponds to the photocurrent, J_0 the saturated reverse current, R_s the series resistance, R_{sh} the shunt resistance, n the ideality factor, and k the Boltzmann constant. The R_s value of the cell with Yb recorded the best results, reaching $1.65 \Omega \text{ cm}^2$, an amount which contributed to a higher FF, compared to the cell with PEIE ($2.02 \Omega \text{ cm}^2$) and LiF ($3.73 \Omega \text{ cm}^2$). It should be noted that the values of R_s and FF can be attributed to the interface properties between the ITO and the active layer, specifically the morphology of the active layer.²³⁻²⁴ In the case of LiF, it was observed that partial

Table 1 Parameters of the Inverted OPV with Different ETLs

| | J_{sc} [mA/cm ²] | V_{oc} [V] | FF | PCE [%] | R_s [$\Omega \text{ cm}^2$] | R_p [$\Omega \text{ cm}^2$] |
|------|-----------------------------------|-----------------|------|------------|------------------------------------|------------------------------------|
| Yb | 10.32 | 0.60 | 0.67 | 4.15 | 2.12 | 1423.00 |
| PEIE | 9.71 | 0.59 | 0.63 | 3.61 | 2.35 | 1518.60 |
| LiF | 7.54 | 0.56 | 0.54 | 2.27 | 5.20 | 587.55 |

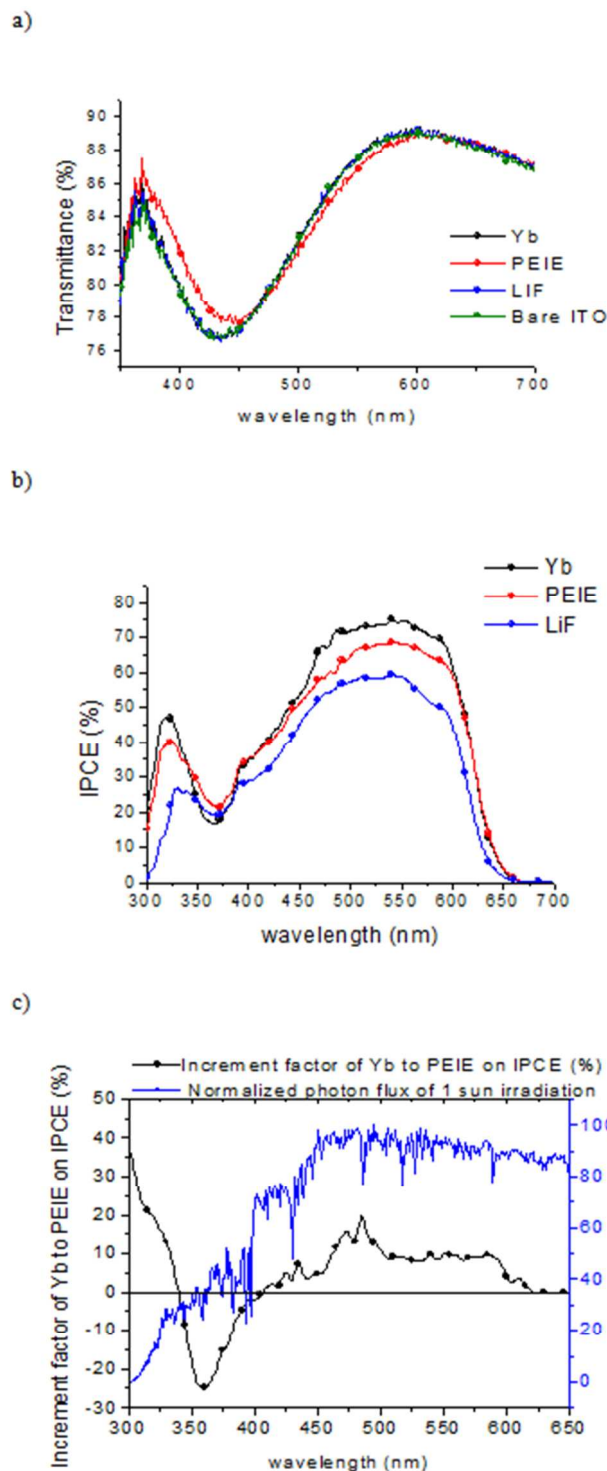


Fig. 3 (a) The transmittance of ETLs (Yb, PEIE, LiF) compared to bare ITO (b) IPCE of the inverted OPVs with different ETLs (c) Increment factor of Yb to PEIE on IPCE and Normalized photon flux of 1 sun irradiation

LiF islands formed on the surface of the ITO when applied with extremely thin thicknesses.¹⁹ These islands indicate that the ITO was not fully covered with LiF when an extremely thin layer of LiF was evaporated on the surface of the ITO. These islands are detrimental

to the performance of the OPVs as the regions which are partially not covered with LiF act as short pathways, resulting in decreases in the R_p . In addition to decreasing the R_p , these islands cause high values of surface roughness (rms), which lead to increases in the R_s due to the increases in contact resistance between the ITO and the active layer. We confirmed these observations via AFM imaging of the surfaces of the different ETLs (see ESI, Fig. S6). As shown in the AFM images (see ESI, Fig. S6), it is clear that the Yb is densely packed on the surface of the ITO. In contrast, the LiF had many void fractions on the surface of the ITO. The roughness of the LiF (3.417 nm) on the ITO was also seen to be 1.85 times higher than that of the Yb (1.84 nm). This implies that the Yb is more inclined for distribution on the surface of the ITO than the LiF. This property indirectly explains that the relatively poor performance of LiF compared to that of Yb. The void fraction of the LiF-coated surface causes short circuiting between the anode and the cathode which leads to low values of R_p .

Optical properties in inverted OPVs with various ETLs

We measured the transmittance of each ETL on the ITO to investigate the influence of how optical loss on J_{sc} . While PEIE on the ITO absorbed light only marginally in the range from 450 nm to 600 nm, Yb and LiF on the ITO barely affected the transmittance of the overall range of the wavelength, a result which is nearly identical to that of the transmittance of bare ITO regardless of thicknesses. (Fig. 3(a)) This implies that metallic elements such as Yb and LiF cause photons to reach the active layer efficiently at 450 nm to 600 nm. The incident photon-to-current conversion efficiency (IPCE) results further support the high efficiency of Yb in minimizing optical loss (Fig. 3(b)). The trends in the IPCE are also similar to those in the transmittance of Yb and PEIE as the IPCE of Yb is higher in the range from 420 nm to 600 nm while PEIE is more transparent in the range from 350 nm to 450 nm. To further elucidate the efficiency of the IPCE of the device with Yb, we calculated the increment factor of the cell with Yb and compared the results to those of cell with PEIE from the IPCE data (Fig. 3(c)). Although the IPCE of the cell with PEIE was 25% higher at 360 nm and generally larger than that of Yb from 330 nm to 420 nm, this increment in PEIE is minor as the amount of spectrum of 1 sun irradiation (blue line in Fig. 3(c)) is relatively small in this range. For the cell with Yb, the IPCE was recorded to be approximately 10% higher in the wide range from 420 nm to 600 nm. In this range of wavelength, the absorbance of the active layer and the amount of 1 sun photon flux were large, contributing to an increase in J_{sc} . In contrast, for the cell with LiF, the IPCE was relatively poor compared to that of cells with Yb and PEIE despite the transparency of LiF which was similar to that of Yb. It should be noted that the transmittance does not directly influence the IPCE. J_{sc} can be described by the equation (2) as below.

$$J_{sc} = \frac{R_{sh}}{R_s} J_0 \left(e^{\frac{q(U_{sc}AR_s)}{nkT}} - 1 \right) \quad (2)$$

The equation above implies that the J_{sc} is not only influenced by the transmittance of ETLs, but also by the values of the R_{sh} and the R_s . Even though LiF has a good level of transparency, its high R_s and

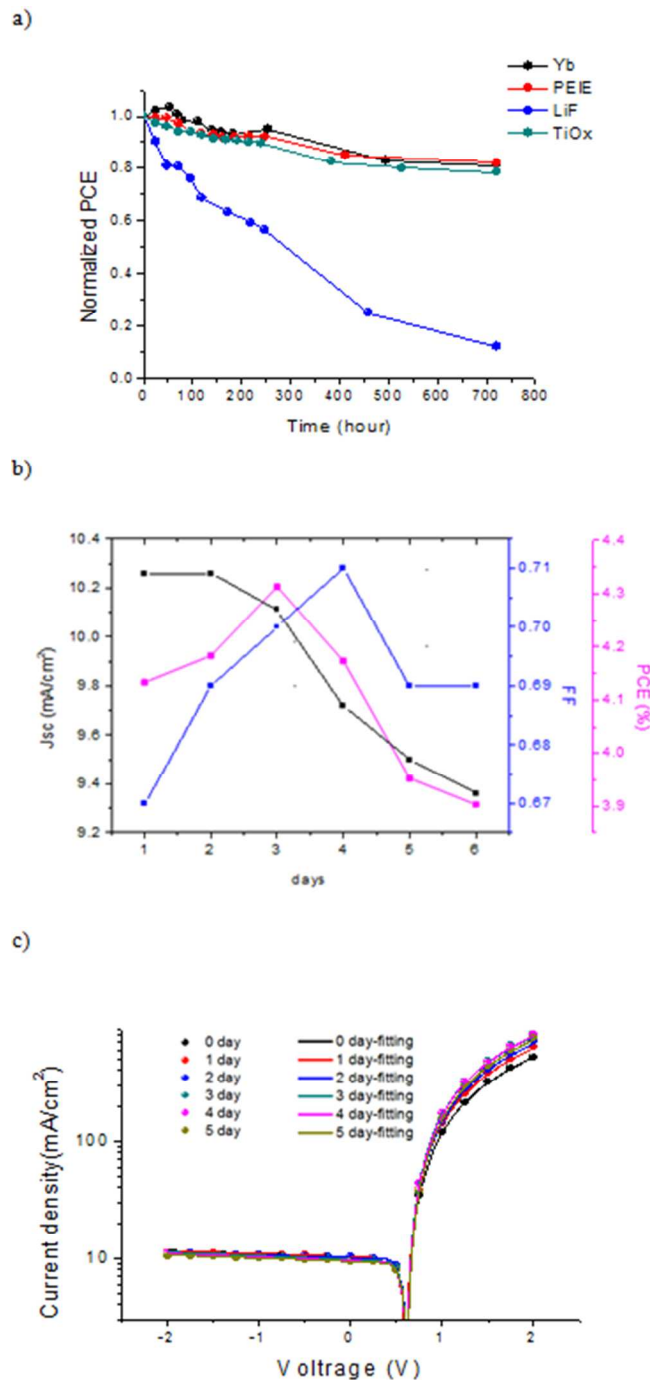


Fig. 4 (a) Normalized PCE of the inverted OPVs incorporating Yb, PEIE and LiF, (b) variation of parameters of the OPV with Yb measured from 0 day to 5 day after the fabrication, (c) logarithmic plot of the J-V curve of the OPV with Yb measured from 0 day to 5 (dot) and data from simulation modeling (line).

small R_p (Table 1) lead to a decrease in J_{sc} , resulting in the poor IPCE. Based on these results, we conclude that the increase in PCE in inverted OPVs with Yb can be attributed to the increase in J_{sc} , small R_s and large R_p which are due to the good transparency values and low roughness of Yb.

Table 2 The Parameters of the Inverted OPVs with Yb Extracted from the Equivalent Circuit Modeling and SSE Method Over Time Elapsed

| | R_s [Ωcm^2] | R_p [Ωcm^2] | $J_0 \cdot 10^{-5}$ [mA/cm ²] | n |
|-------|----------------------------------|----------------------------------|--|------|
| 0 day | 2.12 | 1423.08 | 5.95 | 1.93 |
| 1 day | 2.07 | 1503.11 | 4.12 | 1.87 |
| 2 day | 1.82 | 1664.79 | 3.57 | 1.89 |
| 3 day | 1.58 | 1645.49 | 1.07 | 1.72 |
| 4 day | 1.62 | 1402.89 | 3.07 | 1.86 |
| 5 day | 1.71 | 1530.74 | 4.63 | 1.94 |

Stability in ambient condition

The advantage of using Yb as the ETL of inverted OPVs is not confined to only its improvement in PCE. The inverted OPV with Yb was able to retain 81% of its original PCE even after 30 days. The stability of the inverted OPV with Yb performed comparably well against the inverted OPVs with PEIE and with amorphous titanium oxide (TiOx) which recorded stability levels of 83 % and 79 % of their original PCEs after 30 days respectively (Fig. 4(a)). To confirm the air stability of Yb, we also analyzed conventional OPVs where cathodes are located on the top of the cells. We found that the PCE of the conventional OPV with Yb degraded to 57% of the original value after 260 hours while other conventional OPVs using Ca, LiF degraded completely within 2 days.²⁷ These results imply that Yb itself is not easily oxidized despite its low work function value. It can be concluded that the strong stability of inverted OPVs with Yb is attributed to the structural characteristics of the inverted OPVs, where easily oxidized cathodes are located on the bottoms of the cells, and to the air stability of Yb itself.

Fig. 4(b) shows the change in J_{sc} , FF and PCE of the inverted OPVs with Yb measured from day 0 to day 5 after the fabrication of the OPVs at 1 sun irradiation. Interestingly, the PCE of the cell with Yb increased up to 4.34% after 2 days, a value which is higher than that of the PCE measured immediately after cell fabrication. This phenomenon is contrary to the typical properties of OPVs as most OPVs degrade over time due to the oxidation of the active layer or cathodes regardless of structural differences. In order to extract quantitative information on the inverted OPV with Yb over time, we modelled the data using equation (1) and the sum of the squared errors (SSE) (3) to minimize errors from the raw data measured at 1 sun (Table 2).^{28,29}

$$SSE = \sum [\{ \log(J(V)) - \log(JFIT(V)) \}^2 + \{ J(V) - JFIT(V) \}^2]$$

It can be noted that the FF increased from 67% immediately after cell construction to 71% 3 days afterwards. There was also a slight decrease in J_{sc} as time passed. In regards to the parameters from Table 3, the increase in the FF mostly resulted from the decrease in the R_s . The decrease in the R_s over time is seen in the semilogarithmic plot of the I-V curves (Fig. 4(c)) as the values of the current density were inclined to increase at a forward bias (1V to 2V) from 0 days to 3 days, implying a decrease in the R_s (2.44 $\Omega\text{cm}^2 \sim 1.58 \Omega\text{cm}^2$). Similar to the R_s , the saturated reverse current (J_0)

and the ideality factor (n) also decreased for up to 3 days as shown in Table 2. In contrast to the inverted OPV with Yb, the R_s of most OPVs increased with the degradation of the active layers, interfacial layers, cathodes and anodes as time passed.^{30,31} The J-V curve for the inverted OPV with PEIE over time (see ESI, Fig. S7) supports this observation as the R_s of the inverted OPV with PEIE increased the R_s , leading to a decrease in the FF over time.

In order to identify the mechanism responsible for increasing the FF, we constructed inverted OPVs where the active layer was spin-casted after exposing Yb at ambient air to confirm whether the oxidation of Yb functions to improve the inverted OPVs. As shown in (see ESI, Fig. S8), s-shape curves occurred for the inverted OPVs after the exposure of Yb to oxygen. The s-shape curves were frequently observed in the OPVs with non-optimized active layers and interfacial layers, which were critical factors in the decrease in performance.³²⁻³⁴ Thus, the hypothesis of oxygen exposure to Yb improving inverted OPVs was ruled out. Clear evidence for the improvements over time was difficult to uncover due to limitations in the analysis equipment. However, we indirectly proved that the distribution of the active layer somehow changes on the surface of Yb, which results in these improvements. This is because, generally, the values of J_0 and n are closely related to the morphology of the active layer as the small values of J_0 and n indicate the efficient carrier transport inside the active layer.^{35,36} The analysis to identify how the improvements occur exactly is still under research.

Conclusion

We demonstrated the development of a highly efficient inverted OPV by incorporating Yb as the efficient ETL. Yb outperforms other ETLs such as LiF and PEIE on the PCE. The PCE of the cell with Yb increases from 4.15% to 4.3% 3 days after cell construction. The results also show a decrease in the R_s , J_0 and n, compensating for the gradual decrease in the J_{sc} as time passes. In addition to improvements in the PCE, the stability of the inverted OPV with Yb is comparable to the stability of the inverted OPV with PEIE, recording 81% of its original value after 30 days. The detailed mechanism of Yb was thoroughly analyzed. As a result, we were able to successfully introduce Yb in inverted OPVs to improve the PCE and air stability simultaneously using a basic fabrication technique of evaporating the raw element of Yb onto the ITO.

Acknowledgements

This work was supported by the Human Resource Development program (No.20114010203090) of the Korea Institute of Energy Technology Evaluation and Planning (KETEP) grant funded by the Korea Government Ministry of Trade, Industry and Energy. This work was supported by the Materials and Components Technology Development Business (No. 10046720) of the Korea Evaluation Institute of Industrial Technology (KEIT) grant funded by Korea government Ministry of Trade, Industry and Energy. Sogang University Foundation Research Grants in 2010.

Notes and references

- 1 Z. He, C. Zhong, S. Su, M. Xu, H. Wu, Y. Cao, *Nat. Photon*, 2012, **6**, 591.
- 2 J. You, L. Dou, K. Yoshimura, T. Kato, K. Ohya, T. Moriaty, K. Emery, C.C. Chen, J. Gao, G. Li, Y. Yang, *Nat. Commun*, 2013, **4**, 1446.
- 3 T.D. Neilsen, C. Cruickshank, S. Fogend, J. Thorsen, F.C. Krebs, *Sol. Energy Mater. Sol. Cells*, 2010, **94**, 1553.
- 4 S. K. Hau, H.L. Yip, N.S. Baek, J. Zou, K. O'Malley, A.K.Y. Jen, *Appl. Phys. Lett*, 2008, **92**, 253301.
- 5 T.Y. Chu, S.W. Tsang, J. Zhou, P. G. Verty, J. Lu, S. Beaupre, M. Leclerc, Y. Tao, *Sol. Energy Mater. Sol. Cells*, 2012, **96**, 155.
- 6 M.T. Lloyd, C.H. Peters, A. Garcia, I.V. Kauvar, J.J. Berry, M.O. Reese, M.D. McGehee, D.S. Ginley, D.C.Olsan, *Sol. Energy Mater. Sol. Cells*, 2011, **95**, 1382.
- 7 B. Zimmermann, U. Wurfel, M. Niggemann, *Sol. Energy Mater. Sol. Cells*, 2009, **93**, 491.
- 8 R. Steim, S.A. Choulis, P. Schilinsky, C.J. Brabec, *Appl. Phys. Lett*, 2008, **92**, 093303.
- 9 J.C. Wang, W.T. Weng, M.Y. Tsai, M.K. Lee, S.F. Horng, T.P. Perng, C.C. Kei, C.C. Yu, H.F. Meng, *J. Mater. Chem*, 2010, **20**, 862.
- 10 C. Waldauf, M. Morana, P. Denk, P. Schilinsky, K. Coakley, S.A. Choulis, C.J. Brabec, *Appl. Phys. Lett*, 2006, **89**, 233517.
- 11 J.C. Wang, C.Y. Lu, J.L. Hsu, M.K. Lee, Y.R. Hong, T.P. Perng, S.F. Horng, H.F. Meng, *J. Mater. Chem*, 2011, **21**, 5723.
- 12 C.E. Small, S. Chen, J. Subbiah, C.M. Amb, S.W. Tsang, T.H. Lai, J.R. Reynolds, F. So, *Nat. Photon*, 2012, **6**, 115.
- 13 K. Zilberberg, A. Behrendt, M. Kraft, U. Scherf, T. Riedl, *Org. Electron*, 2013, **14**, 951.
- 14 H. Kang, S. Hong, J. Lee, K. Lee, *Adv. Mater*, 2012, **24**, 3005.
- 15 Y. Zhou, C.F. Hernandez, J. Shim, J. Meyer, A.J. Giordano, H. Li, P. Winget, T. Papadopoulos, H. Cheun, J. Kim, M. Fenoll, A. Dindar, W. Haske, E. Najafabadi, T.M. Khan, H. Sojoudi, S. Barlow, S. Graham, J.L. Bredas, S.R. Marder, A. Kahn, B. Kippelen, *Science*, 2012, **336**, 6079.
- 16 G. Li, V. Shrotriya, Y. Yao, J. Huang, Y. Yang, *J. Mater. Chem*, 2007, **17**, 3126.
- 17 R.B. Aich, Y. Zou, M. Leclerc, Y. Tao, *Org. Electron*, 2010, **11**, 1053.
- 18 A.F. Shestakov, M.A. Katkova, N.S. Emel'yanova, T.V. Balashova, V.A. Il'ichev, A.N. Konev, D.M. Kuzyaev, V.A. Lopatin, M.N. Bochkarev, *High Energy Chemistry*, 2010, **44**, 503.
- 19 Y.J. Lee, X. Li, D.Y. Kang, S.S. Park, J. Kim, J.W. Choi, H. Kim, *Ultramicroscopy*, 2008, **108**, 1315.
- 20 S. Zhu, J. Chen, M.F. Li, S. J. Lee, J. Singh, C. X. Zhu, A. Du, C.H. Tung, A. Chin, D.L. Kwong, *IEEE Electron Dev. Lett*, 2004, **25**, 565.
- 21 M.T. Greiner, M.G. Helander, W.M. Tang, Z.B. Wang, J. Qju, Z.H. Lu, *Nat. Mater*, 2012, **11**, 76.
- 22 Y. Zhou, C.F. Hernandez, J. Shim, J. Meyer, A.J. Giordano, H. Li, P. Winget, T. Papadopoulos, H. Cheun, J. Kim, M. Fenoll, A. Dindar, W. Haske, E. Najafabadi, T.M. Khan, H. Sojoudi, S. Barlow, S. Graham, J.L. Bredas, S.R. Marder, A. Kahn, B. Kippelen, *Science*, 2012, **336**, 6079.
- 23 P. Vanlaeke, A. Swinnen, I. Haeldermans, G. Vanhoyland, T. Aernouts, D. Cheyns, C. Deibel, J. D'Hean, P. Heremans, J. Poortmans, J.V. Manca, *Sol. Energy Mater. Sol. Cells*, 2006, **90**, 2150.
- 24 R.A. Marsh, J.M. Hodgkiss, S.A. Seifried, R.H. Friend, *Nano Lett*, 2010, **10**, 923.
- 25 T.M. Clarke, A.M. Ballantyne, J. Nelson, D.D.C. Bradley, J.R. Durrant, *Adv. Funct. Mater*, 2008, **18**, 4029.
- 26 E. Verploegen, R. Mondal, C.J. Bettinger, S. Sok, M.F. Toney, Z. Bao, *Adv. Funct. Mater*, 2010, **20**, 3519.
- 27 I.S. Oh, G.M. Kim, S.H. Han, A.N. Lee, S.Y. Oh, The conventional OPVs featuring Yb as an n-type buffer layer, not published yet.
- 28 S.H. Yoo, B. Domercq, B. Kipplen, *J. Appl. Phys*, 2005, **97**, 103706.
- 29 C. Zhang, J. Zhang, Y. Hao, Z. Lin, C. Zhu, *J. Appl. Phys*, 2011, **110**, 064504.
- 30 M. Jorgensen, K. Norrman, F.C. Krebs, *Sol. Energy Mater. Sol. Cells*, 2008, **92**, 686.
- 31 N. Grossiord, J.M. Kroon, R. Andriessen, P.W.M. Blom, *Org. Electron*, 2012, **13**, 432.
- 32 J.C. Wang, X.C. Ren, S.Q. Shi, C.W. Leung, P.K.L. Chan, *Org. Electron*, 2011, **12**, 880.
- 33 A. Wagenpfahi, D. Rauh, M. Binder, C. Deibel, V. Dyakonov, *Phys. Rev. B*, 2010, **82**, 115306.
- 34 W. Tress, A. Petrich, M. Hummert, M. Hein, K. Leo, M. Riede, *Appl. Phys. Lett*, 2011, **98**, 063301.

Journal Name

35 C. Waldauf, M. Morana, P. Denk, P. Schillinsky, K. Coakley, S.A. Choulis, C.J. Brabec, *Appl. Phys. Lett*, 2006, **89**, 233517.

36 A. Jain, A. Kapoor, *Sol. Energy Mater. Sol. Cells*, 2005, **85**, 391.